

ARTICLE

Open Access

Biodegradable triboelectric nanogenerator as a implantable power source for embedded medicine devices

Gang Jian¹, Shangtao Zhu¹, Xiao Yuan², Shengqiao Fu², Ning Yang¹, Chao Yan¹, Xu Wang² and Ching-Ping Wong³

Abstract

Implantable medical devices have played an important role in human medicine in recent decades. However, traditional implanted devices require battery replacement and a second surgery for device removal, which can cause pain to the patient. This work presents a biodegradable triboelectric nanogenerator (BI-TENG) made from both natural and synthetic biodegradable materials that is utilized to collect mechanical energy in vivo and transduce it into electricity. Reed film and polylactic acid were chosen among different biodegradable materials as the triboelectric layers due to having the best generator output performance by providing voltages that reached 368 V. The biocompatibility of the friction layer and the device was verified via a blood test. After implantation in mice, the BI-TENG exhibited an open-circuit voltage of 0.176 V and a short-circuit current of 192 nA as generated from body movement. The BI-TENG was connected to an interdigital electrode to generate an electric field, which stimulated the accelerated release of doxorubicin (DOX) from red blood cells in targeted drug delivery systems. After stopping the electric field, the release of DOX normalized, facilitating the precise killing of cancer cells. Our work demonstrates the broad potential of BI-TENGs in the field of cancer treatment.

Introduction

Implantable electronic devices are advantageous electronic devices used in medicine and have played a key role in the field of human medicine in recent decades. However, implantable electronic devices for medical use still have some drawbacks; for example, some implantable devices cannot be self-powered and therefore need a battery; other implantable devices require secondary surgery to remove them after use, which imposes a financial burden and severe pain on patients. Thus, implantable electronics that degrade harmlessly in the

human body are particularly important. Such biodegradable implants should work in human tissue without being rejected by the body. In general, medical devices have begun to play an important role in the diagnosis and treatment of certain medical procedures^{1–9}. Researchers have performed much work on various electronic devices for in vivo sensors and therapeutics^{10–18}. In the field of biomedicine, triboelectric nanogenerators (TENGs) are emerging as novel potential energy sources for implanted devices that eliminate microorganisms in tissue layers¹⁹, accelerate wound healing¹² and provide ultrasound mechanical energy harvesting²⁰.

Chemotherapy is the most commonly used treatment for cancer, and doxorubicin (DOX) is a widely accepted chemical drug. Moreover, chemotherapy has severe side effects; for example, patients may develop drug resistance after a long period of chemotherapy to decrease the therapeutic efficacy. To minimize chemotherapeutic

Correspondence: Gang Jian (gjian@just.edu.cn) or

Xu Wang (wangxu@ujs.edu.cn) or

Ching-Ping Wong (cp.wong@mse.gatech.edu)

¹School of Materials Science and Engineering, Jiangsu University of Science and Technology, Zhenjiang 212100, China

²Department of Radiation Oncology, Institute of Oncology, Affiliated Hospital of Jiangsu University, Zhenjiang 212013, China

Full list of author information is available at the end of the article

© The Author(s) 2024



Open Access This article is licensed under a Creative Commons Attribution 4.0 International License, which permits use, sharing, adaptation, distribution and reproduction in any medium or format, as long as you give appropriate credit to the original author(s) and the source, provide a link to the Creative Commons licence, and indicate if changes were made. The images or other third party material in this article are included in the article's Creative Commons licence, unless indicated otherwise in a credit line to the material. If material is not included in the article's Creative Commons licence and your intended use is not permitted by statutory regulation or exceeds the permitted use, you will need to obtain permission directly from the copyright holder. To view a copy of this licence, visit <http://creativecommons.org/licenses/by/4.0/>.

efficacy, targeted drug delivery systems (DDSs) have been developed accordingly, and great progress has been made in recent decades with continuous efforts from researchers. When using such systems, due to the discontinuity of neoplastic endothelial cells, particles of a certain size can reach the tissue space through the vascular wall through the enhanced permeability and retention effect (EPR) of the tumor, i.e., the high permeability and retention effect of the solid tumor. Therefore, researchers have focused on carriers and nanoparticles for use in DDS systems^{21,22}, such as micelles²³, nanoparticles²⁴, microcapsules²⁵ and nanogels²⁶. However, these carriers and nanoparticles still possess certain biological toxicity and cannot accurately deliver drugs; thus, they are rarely used in actual medical procedures. In contrast, red blood cells (RBCs), have a wide range of sources, a long half-life of 120 days, good biocompatibility, membrane flexibility and stability^{27–29}. The effective size range of EPR is generally 300 nm–4.7 μm ³⁰, and the diameter of erythrocytes is within this range. Furthermore, the membranes of red blood cells are flexible and able to penetrate the tumor site. By using surface ligands and magnetic nanoparticles, medications can be administered more precisely to the tumor location^{31,32}.

The purpose of DDSs is to deliver more drug to the tumor area rather than depositing it in healthy regions of the body and thereby causing harm. Stimulation through an electric field (EF) is also an excellent treatment option^{33–35} because an electric field exhibits minimal harm to the human body, is simple to operate, and has a low cost to administer^{36,37}. An implantable TENG could be used in a DDS system to generate an electric field. In this study, we designed a biodegradable triboelectric nanogenerator (BI-TENG) for cancer treatment.

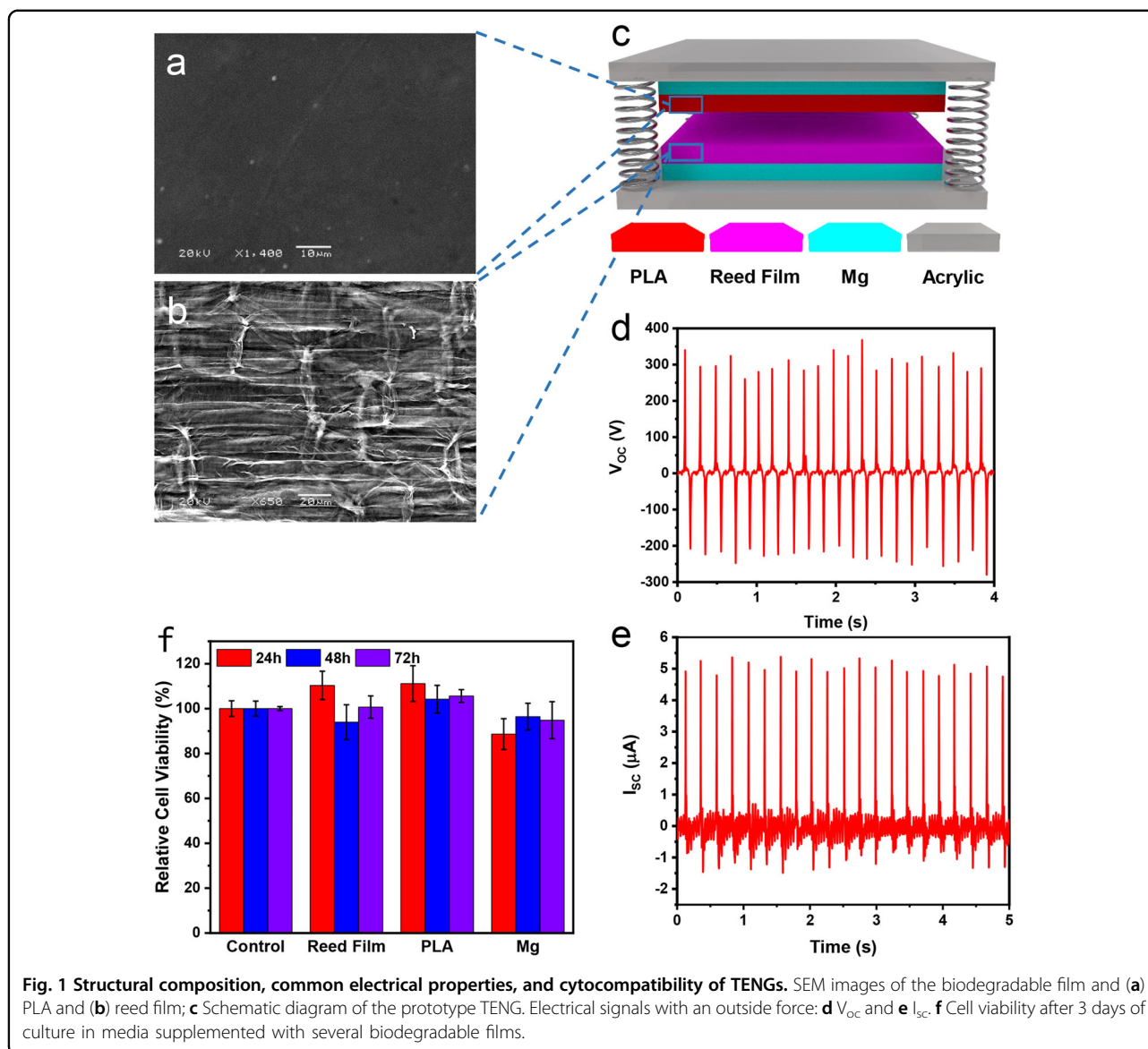
Our BI-TENG generates an electric field after implantation to drive DDS for cancer treatment. Two different biodegradable materials were selected to prepare a BI-TENG, which was implanted into mice, and a relatively stable output was obtained. A BI-TENG was used to generate an electric field to control DOX loading and release from RBCs in a simulated tumor cell environment. Under normal conditions, DOX-loaded erythrocytes release drugs. In addition to the increase in EF produced by the BI-TENG, the release of erythrocytes was accelerated. The results revealed that the DDS driven by the BI-TENG has a remarkable killing effect on tumors.

Results and discussion

BI-TENGs were prepared using biodegradable materials^{38,39}. Other features of the materials used to prepare BI-TENGs include good adaptability to biological environments, compatibility with a variety of polymer operations, and preferably, already been used in medicine. Furthermore, the two materials used as friction layers should have

different electron-gain and electron-loss capabilities for TENGs⁴⁰. Due to these requirements, polylactic acid (PLA), a synthetic polymeric material, and reed membrane, a natural material, were selected as the positive and negative friction materials, respectively, for the BI-TENG. PLA has been adopted for several reasons. First, PLA is made from starch derived from natural plant resources such as maize⁴¹. Glucose is produced from unprocessed starch sources through glycation. Glucose was fermented by the specified strains to create high-purity lactic acid via the chemical synthesis of polylactic acid at a particular molecular weight (Fig. S1). The molecular structural formula of PLA is shown in Fig. S2. After use, PLA can be entirely degraded by microorganisms in the environment, releasing safe products of carbon dioxide and water, which environmentally friendly and biocompatible. Moreover, PLA is a biomedical material used in the creation of disposable infusion devices, absorbable sutures, and low-molecular-weight packaging substances for drugs with sustained release⁴². In addition, PLA has excellent antibacterial and antifungal functions. Reed film is a natural plant material derived from reeds. Its main component is cellulose, the molecular structure of which is shown in Fig. S3. It comes from a variety of sources and can be naturally degraded. The cytoderm of the reed membrane was elongated, with an average width of $\sim 43.4 \mu\text{m}$ (Fig. S4).

As shown in Fig. 1c, a prototype TENG was prepared with a vertical contact/separation working mode^{43–47}. In addition to the friction layers and electrode layers, there are substrates and spacers inside the nanogenerator, which possesses an active size of 5 cm \times 5 cm. An acrylic plate was used as the substrate, PLA and reed films were used as the friction layers of the BI-TENG, and a magnesium (Mg) film was attached to each friction layer as the conductive electrode. Pulsed forces generated by a mechanical linear motor were applied to monitor the electrical performance of the TENG. At a frequency of 5 Hz, the open-circuit voltage reaches 368 V (Fig. 1e), and the short-circuit current reaches 5.37 μA (Fig. 1f). The as-prepared TENG is inversely connected to the electrometer, and the outputs obtained are displayed in Fig. S5. The directions of the open-circuit voltage and short-circuit current are completely opposite, proving that the output is entirely governed by the TENG. To investigate the impedance properties of the TENG, resistors with different values were connected for testing. As shown in Fig. S6, the voltage on the load increases with increasing load resistance, whereas the current continues to decrease. This phenomenon occurs due to the occurrence of ohmic loss. The figure also demonstrates that the output power density is a maximum of 0.256 W m^{-2} when the resistance is 10 M Ω . Figure S6 indicates that the voltage generated by TENGs is frequency dependent. The



output power generated by the TENG can be used to charge a commercial capacitor, and the corresponding charging curve is shown in Fig. S7. The device can charge the capacitor to 0.727 V within 140 s. Figure S8 shows that the TENG can power 60 red LED lights (Movie S1) without needing a capacitor. The results demonstrated that the created TENG is effective at transforming mechanical energy into electrical energy. Furthermore, at a constant frequency, the TENG showed excellent stability after 10,000 cycles of testing (Fig. S9).

To evaluate the biological safety of the PLA and reed membranes, mouse colon cancer cell (i.e., MC38) culture experiments were conducted with the PLA and reed membrane, respectively. As shown in Fig. 1f, after 24, 48 and 72 h of culture, the survival rate of cells cultured on the PLA reed membrane and Mg remained high, and the

fluctuations in cell activity in the figure were caused by fluctuations in the cell growth rate in the control group. Direct observation of the OD measured by the enzyme-labeling agent showed that the cells grew well from these materials (Fig. S10). These results suggest that these two materials are healthy and harmless to most organisms, including cancer cells, before they can be made into TENGs.

The power generation process of the BI-TENG occurs through contact and separation between the two friction layers, and the mechanical energy of the extruded BI-TENG is converted into electrical output through the interaction of the electrostatic inductor with the triboelectric effect^{48–50}. As shown in Fig. 2a, under extrusion pressure, the two friction materials contact each other. Due to the different capabilities of the materials for

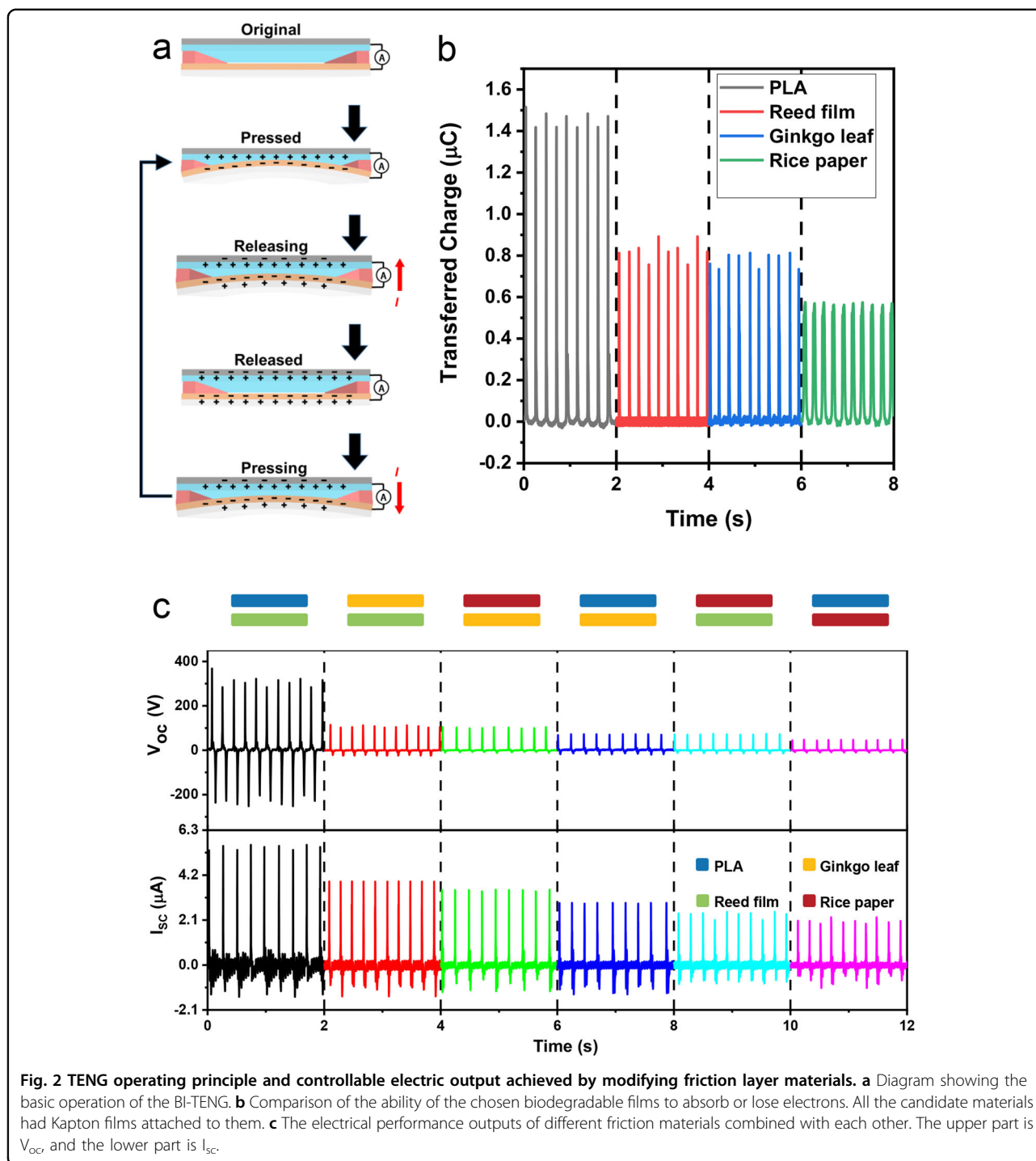
absorbing and losing electrons, electrons and holes are present on the surfaces of the two friction materials. When the external extrusion pressure is released, the two friction materials are separated. To maintain the electrostatic balance between them, free electron extension wires on the conductive electrode are transferred, forming a current that conducts until the original states of the two friction materials are completely recovered, at which point the current decreases to zero. Under the action of extrusion pressure, the two friction materials gradually contact each other, producing a current of equal magnitude and opposite direction, resulting in an alternating electrical signal output in the circuit.

To illustrate the advantages of the selected friction materials, in addition to PLA and reed film, two biodegradable materials, rice paper and ginkgo biloba, were compared for their performance as TENGs. Scanning electron microscopy (SEM) images of the rice paper and ginkgo biloba powders are shown in Fig. S11. The surface of the rice paper has a large number of small grain protrusions, while the powder on the ginkgo biloba leaves has a large grain. The corresponding Fourier transform infrared (FTIR) spectra shown in Fig. S12 confirm the phases of each material. Specifically, the characteristic vibrations of the methyl and carbonyl groups in PLA are represented by peaks at 2925 cm^{-1} and 1754 cm^{-1} (Fig. S12a), respectively. The stretching vibrations of O–H and C–H and the asymmetric stretching vibration of C–O–C are illustrated by the peaks at 3364 cm^{-1} , 2914 cm^{-1} , and 1061 cm^{-1} , respectively (Fig. S12b). For the rice paper, the distinctive protein amide peaks are located at 1643 cm^{-1} and 1373 cm^{-1} (Fig. S12c). The asymmetric stretching vibrations of the C–O–C groups in Ginkgo biloba are represented by the peak at 1015 cm^{-1} (Fig. S12d). Figure S13 shows the X-ray diffraction (XRD) images of the four materials, which confirm the material phases. Figure S14 shows the water contact angles of the different materials. When the water contact angle is less than 90° , the material shows excellent hydrophobicity, which is beneficial for the degradation of these materials.

The performance output of a TENG is related to its ability to gain and lose electrons. PLA, reed film, rice paper and ginkgo biloba were used as friction material layers for the TENG, and Kapton was used as the other friction layer. The power generation of each group was measured, and the values were compared and sorted. The final results were as follows: PLA > reed film > ginkgo biloba > rice paper (Fig. 2b); these results can be regarded as “triboelectric series”^{51,52}. With the guidance of the triboelectric series, PLA, reed film, rice paper and ginkgo biloba were combined to prepare TENGs ($5 \times 5\text{ cm}^2$). A comparison of the open-circuit voltage and short-circuit current produced by these materials (Fig. 2c) revealed that

the TENG composed of PLA and reed film exhibited the best electrical performance.

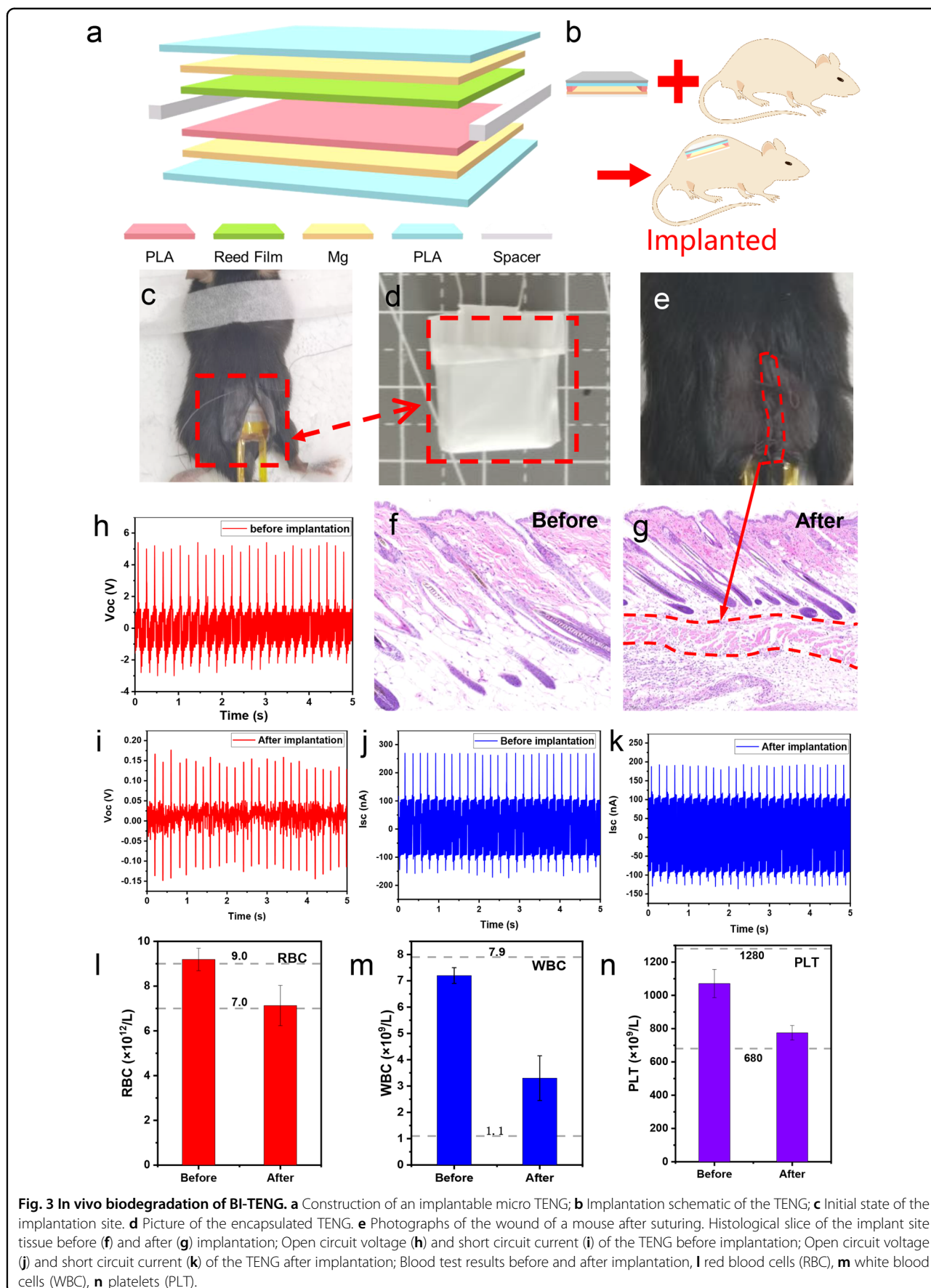
A small BI-TENG constructed from the prototype TENG was fabricated to demonstrate the in vivo implantable medical performance (Fig. 3a). To ensure that the BI-TENG was fully biodegradable, the substrate material was also selected as the biodegradable material. PLA was ultimately selected as the substrate material due to its excellent properties. To isolate the interference of the external environment on the performance of the device, PLA was used as the encapsulation layer of the BI-TENG. The various materials for preparing the BI-TENG were added to PBS to simulate the in vivo environment, and after a period of time, it was observed that the BI-TENG underwent obvious degradation (Fig. S15). PLA clearly degraded after 30 days, and the Mg and reed films obviously degraded after 1 day and 3 days, respectively. Figure 3d shows a photograph of the small BI-TENG that was prepared. The small BI-TENG was sterilized with 75 vol% alcohol and implanted subcutaneously into mice (Fig. 3c). The experiment was carried out in strict accordance with the national standard “Requirements for Laboratory Animal Environment and Living Facilities (GB 14925-2001)”. Figure 3c shows the process of TENG implantation under the skin of mice, while Fig. 4f shows photographs of the wounds sutured from the mice after TENG implantation. Figure 3f, g shows histological sections of two different mice pre- and postimplantation, revealing that the BI-TENG was situated between the muscular tissue and the dermal tissue. No obvious inflammatory conditions were found, which indicated the good biocompatibility of the BI-TENG. The electrical performance of TENGs is important for their implantation. To prevent the mice from biting the surgical wound after the operation, the site of TENG implantation was tapped while the mice were anesthetized. The open-circuit voltage of the TENG was 0.176 V (Fig. 3i), and the short-circuit current was 190 nA (Fig. 3k). A comparison of the open-circuit voltage and short-circuit current before implantation (Fig. 3h, j) revealed a decrease in performance, which is attributed to compression of the mouse tissue surrounding the BI-TENG, which limited the movement of the TENG. Moreover, to determine the service lifetime of the BI-TENG in vivo, the device was placed in a PBS solution, the environment was simulated in vivo, and a reliability experiment was carried out. The device still maintained good performance after 8000 operations (Fig. S16). To study whether the mice rejected after TENG implantation, blood samples were collected before and 2 days after TENG implantation for a standard blood test, and the percentages of red blood cells, white blood cells and platelets before and after TENG implantation were compared. The results are shown in Fig. 3l, m. The concentrations of red blood cells, white blood cells

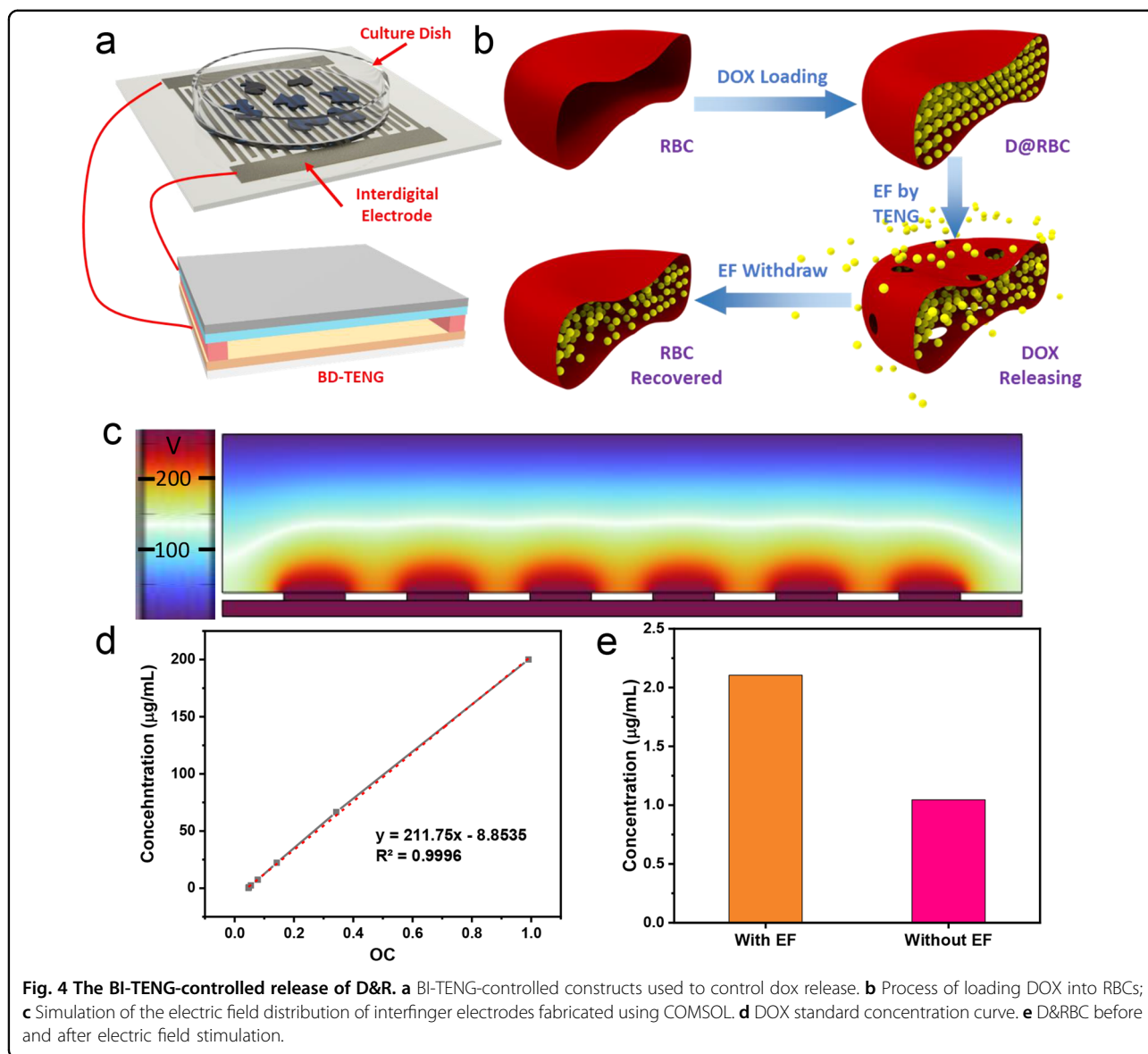


and platelets in the implanted mice were reduced but still within the normal range, indicating that the mice did not experience anemia or inflammatory reactions after the operation.

DOX was then loaded into erythrocytes by hypoosmotic chromatography. The red blood cell suspension and DOX solution at a dose of $200 \mu\text{g ml}^{-1}$ were mixed together, in

which glutathione (GSH) and adenosine triphosphate (ATP) were added to prevent oxidation of the cytomembrane and maintain the intact structure of the cytomembrane. The plants were then maintained at 4°C to inflate the red blood cells and allow DOX to enter them. These DOX-loaded red blood cells were subsequently washed, transferred to hypertonic buffer, and incubated at





37 °C to restore the internal and external osmotic pressure of the red blood cells and restore the cell membrane. After DOX loading, the DOX-loaded red blood cell suspension was added to the culture dish containing the cancer cells, and interdigital electrodes with a width of 100 µm and spacing of 100 µm were placed at the bottom of the dish, as shown in Fig. 4a. These interdigital electrodes were driven by the TENG to generate an EF, which stimulates the erythrocyte membrane to generate electricity to perforate and accelerate the release of the DOX. This release returned to normal after EF removal (Fig. 4b). The modeling of the electric field produced by the BI-TENG is shown in Fig. 4c. To determine the effect of EF on DOX release from loaded RBCs, standard curves of DOX concentration (Fig. 4d) were prepared using different concentrations of the DOX in a PBS. After the electric field

stimulation of D&RBC for half an hour, the supernatant was collected before and after electric field stimulation, and the DOX concentrations before and after stimulation were calculated (Fig. 4e). The amount of DOX released by D&R-treated cells after electric field stimulation was significantly greater than that released without stimulation.

The survival outcomes of cancer cells in different environments were compared. Cancer cells were incubated with free red blood cells, DOX-loaded red blood cells, or free DOX (20 µg ml⁻¹) for half an hour. After incubation, the cells were divided into two groups: one group was left untreated, and the other group was stimulated with TENG-driven EFs. After that, the cells were cultured at 37 °C for 24, 48, or 72 h, and a cell counting kit-8 (CCK-8) assay was performed to determine the activity of the cancer cells. The results are shown in Fig. 5a–f. During the

experiment, care was taken so that the medium was not contaminated with bacteria; otherwise, deterioration occurred (Fig. S19). Treatment of cancer cells with EF alone, RBC alone, or a combination of the two agents did not significantly change survival (Fig. 5g), with slight variation possibly due to differences in the daily changes among the groups. Changes in the activity of cancer cells treated with free DOX and EF+ free DOX were evident (Fig. 5h). Although the cell survival rate of the D&RBC group was not as high as that of the DOX group (which is attributed to the lower concentration of DOX released by D&RBC than by the DOX group), there was a clear trend toward a lower cell survival rate. After applying the electric field, the release of DOX increased, and the killing effect on cancer cells improved. Figure 5i–p shows the micrographs of the treated groups, and the results generally agree with the measured data. In the RBC, RBC + EF, D&RBC and D&RBC + EF groups, many small particles (indicated via blue circles), which are red blood cells, were observed. In the control, EF, RBC and RRBC + EF groups, intact cancer cells (indicated via red circles) were observed, and in the DOX and DOX + EF groups, the cancer cells were completely killed, leaving behind the cancer cells. In the D&RBC and D&RBC + EF groups, although the cancer cells did not die completely, their activity also decreased significantly, and the cells were in a dying state. Among them, the number of cells in the D&RBC + EF group was significantly lower than that in the D&RBC group. Thus, D&RBC + EF had an excellent inhibitory effect on cancer cells.

Conclusion

In summary, we investigated four biodegradable materials and evaluated their friction capabilities. The two best triboelectric series were adopted to fabricate a BI-TENG that takes advantage of an organism's mechanical energy and transforms it into electricity. The BI-TENG showed outstanding performance, with an open-circuit voltage reaching 0.176 V and a short-circuit current reaching 190 nA after implantation. Moreover, in addition to offering good biocompatibility and degradability in the body, these materials greatly reduce patient pain. DDSs were developed to accurately deliver drugs to tumors and exert their effects while controlling medication release at the ideal time and place. The BI-TENG was used as the power source to stimulate the electric field to increase the speed of the DDS system release of DOX from RBCs, and the DOX release rate returned to normal after the applied field was stopped. In this way, the damage to the human body during cancer treatment is reduced, and the killing efficiency of cancer cells is improved. In view of the good biocompatibility, degradability and output performance of BI-TENGs, the BI-TENG proposed in this study has a wide range of cancer treatment applications.

Materials and methods

Preparation of the BI-TENG based on PLA and reed film

The PLA and reed films used as friction layer materials were cut into squares with an area of 1 cm × 1 cm; both were attached to the Mg film as a conductive electrode, and a wire was drawn at the conductive electrode. For the material to be degradable, both the substrate and encapsulation material must be degradable, so PLA is still used. PLA, which was used as the encapsulation material, was sealed using a heat sealing machine to avoid interference from the experimental results with the mouse tissue fluid.

Characterization

SEM images were captured with a tungsten filament scanning electron microscope (JEOL JSM6480). X-ray diffraction (XRD) was performed using an X-ray diffractometer (XRD-6000, SHIMADZU). All FTIR spectra were collected with a Fourier transform infrared spectrometer (NICOLET IS10, Thermo Fisher). All voltages, transferred charges and currents were measured by an electrometer (Ke6514, Keithley) and recorded by an oscilloscope (TBS1072B, Tektronix) or data acquisition hardware (USB-6002, National Instruments). Cell viability was assessed and quantified using a microplate reader (ELX800, Biotek), and the results were calculated.

In vitro electrical properties of the BI-TENG

Mechanical measurements of the electrical properties of the BI-TENG were performed with a linear motor system that delivered a periodic compressive force with a 5 Hz frequency. To analyze the output V_{oc} , a digital oscilloscope (Tektronix, TBS1072B, USA) was used. An electrometer (Keithley, 6514, USA) was used to measure both the output I_{sc} and the transferred charges (Fig. S17).

In vivo implantation and test of the BI-TENG

Prior to implantation surgery, the BI-TENG and all surgical tools were disinfected using cleaning solution containing 75% alcohol. Chloral hydrate (5%) was injected through the abdomen to make the mice unconscious. The sterilized BI-TENG was implanted into the subcutaneous area of the back of the mouse, where it was easy to observe. During the measurement of electrical signals, the mice were prevented from biting the wound, and the implanted BI-TENG was actuated by applying an external force by tapping the skin of the implanted site with a finger. A digital oscilloscope was used to characterize the output electrical performance (Movie S2 and Fig. S18).

Cell culture

MC38 cells (Affiliated Hospital of Jiangsu University, Jiangsu, China) were cultured in DMEM supplemented with 10% serum at 37 °C in a 5% CO₂ atmosphere in a CO₂ incubator. After incubating for a certain time, the

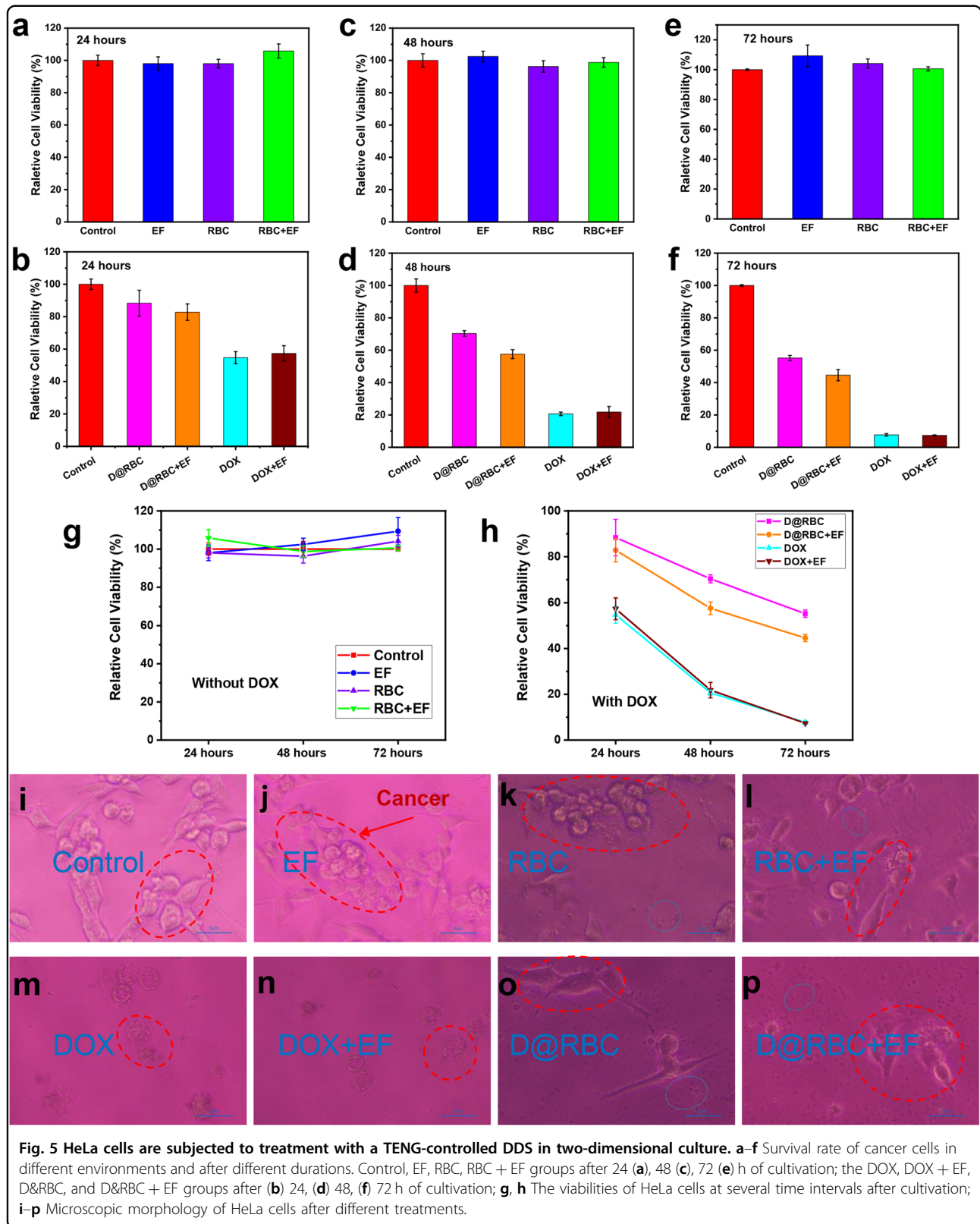


Fig. 5 HeLa cells are subjected to treatment with a TENG-controlled DDS in two-dimensional culture. **a–f** Survival rate of cancer cells in different environments and after different durations. Control, EF, RBC, RBC + EF groups after 24 (**a**), 48 (**c**), 72 (**e**) h of cultivation; the DOX, DOX + EF, D&RBC, and D&RBC + EF groups after (**b**) 24, (**d**) 48, (**f**) 72 h of cultivation; **g, h** The viabilities of HeLa cells at several time intervals after cultivation; **i–p** Microscopic morphology of HeLa cells after different treatments.

culture dish media was removed, and PBS (1×) was used to rinse the cells. The cells were added to a PBS solution containing 1–2 mL of trypsin and then processed for 2 min in an incubator at 37 °C. Digestion was stopped with two times as much trypsin in complete medium, 2–4 ml of complete medium was used to resuspend the cells after being washed three times with PBS solution and diluted to 4000 cells/100 µl, after which the cells were seeded in 96-well plates. MC38 cell proliferation was detected via a microplate reader.

Calculation of relative cell viability

The normalized data reduction method is as follows:

$$\overline{M_C} = \frac{\sum_1^n M_{Cn}}{n} \quad (1)$$

$$\overline{M_E} = \frac{\sum_1^n M_{En}}{n} \quad (2)$$

$$\overline{RCV_C} = \frac{\overline{M_C}}{\overline{M_C}} \quad (3)$$

$$\overline{RCV_B} = \frac{\overline{M_E}}{\overline{M_C}} \quad (4)$$

where M_C is the average value of the data gathered from the control group and M_E is the average value of the data gathered from the experimental group. RCV_C was used to normalize cell viability in the control group, and RCV_E was used to normalize cell viability in the experimental group.

Preparation of D&R

D&RBC were prepared using the classical hypotonic method⁵³ by first taking whole blood from mouse eye sockets. The blood sample was placed in a centrifuge at 3000 rpm min⁻¹ for 5 min to separate the red blood cells from the sample. Then, the red blood cells were washed three times with cold PBS solution, and 70% PBS was added to prepare a red blood cell suspension. Hypotonic buffer was prepared by adding 200 µg ml⁻¹ DOX and 3 × 10⁻³ M glutathione (98%, Aladdin, China) to 70% PBS. Then, 1 ml of hypotonic buffer was added to the RBC suspension and incubated for 40 min at 4 °C. After loading, the cells were placed in a centrifuge, shaken at 3000 rpm for 5 min, and resuspended in PBS. The solution was added to 130% PBS containing 3 × 10⁻³ M glutathione, 100 × 10⁻³ M sodium pyruvate (99%, Aladdin, China), and 100 × 10⁻³ M inosine (98%, Aladdin, China). The cells were incubated at 37 °C for 40 min to restore intracytoplasmic and intracytoplasmic osmotic pressure.

Extra DOX was eliminated by flushing the cells four times with cold PBS solution.

Acknowledgements

This work was supported by the National Natural Science Foundation of China (51873083, 32170910), the Natural Science Foundation of Jiangsu Province (BK20211124), the Industry University Research Cooperation Project in Jiangsu Province (BY2020679, BY2021522) and the Graduate Practice and Innovation Projects in Jiangsu Province (SJCX22_1937).

Author details

¹School of Materials Science and Engineering, Jiangsu University of Science and Technology, Zhenjiang 212100, China. ²Department of Radiation Oncology, Institute of Oncology, Affiliated Hospital of Jiangsu University, Zhenjiang 212013, China. ³School of Materials Science and Engineering, Georgia Institute of Technology, Atlanta, GA 30339, USA

Author contributions

G.J.: conceptualization, investigation, formal analysis, writing—original draft, writing—review and editing. S.Z.: methodology, data curation, formal analysis, writing—original draft. X.Y.: methodology. S.F.: methodology. N.Y.: project administration. C.Y.: formal analysis. X.W.: supervision, project administration. C.-P.W.: conceptualization, supervision.

Data availability

The data of this study are available from the corresponding authors upon reasonable request.

Competing interests

The authors declare no competing interests.

Publisher's note

Springer Nature remains neutral with regard to jurisdictional claims in published maps and institutional affiliations.

Supplementary information The online version contains supplementary material available at <https://doi.org/10.1038/s41427-023-00528-2>.

Received: 8 August 2023 Revised: 10 December 2023 Accepted: 14 December 2023

Published online: 01 March 2024

References

- Bettinger, C. J. & Bao, Z. Organic thin-film transistors fabricated on resorbable biomaterial substrates. *Adv. Mater.* **22**, 651–655 (2010).
- Irimia-Vladu, M. et al. Biocompatible and biodegradable materials for organic field-effect transistors. *Adv. Funct. Mater.* **20**, 4069–4076 (2010).
- Li, C. et al. Design of biodegradable, implantable devices towards clinical translation. *Nat. Rev. Mater.* **5**, 61–81 (2020).
- Li, Z., Zhu, G., Yang, R., Wang, A. C. & Wang, Z. L. Muscle-driven in vivo nanogenerator. *Adv. Mater.* **22**, 2534–2537 (2010).
- Omenetto, F. G. & Kaplan, D. L. New opportunities for an ancient material. *Science* **329**, 528–531 (2010).
- Tian, B. et al. Coaxial silicon nanowires as solar cells and nanoelectronic power sources. *Nature* **449**, 885–889 (2007).
- Kim, D.-H. et al. Materials for multifunctional balloon catheters with capabilities in cardiac electrophysiological mapping and ablation therapy. *Nat. Mater.* **10**, 316–323 (2011).
- Mahapatra, S., Kumari, R., Dkhar, D. S. & Chandra, P. Engineered nanomaterial based implantable micronanoelectrode for in vivo analysis: technological advancement and commercial aspects. *Microchem. J.* **187**, 108431 (2023).
- Luo, R. et al. Reshaping the endogenous electric field to boost wound repair via electrogenerative dressing. *Adv. Mater.* **35**, 2208395 (2023).
- Bao, Z. & McCulloch, I. Organic field-effect transistors IX. *Proc. SPIE Int. Soc. Opt. Eng.* **18**, 121–136 (2010).

11. Wang, T. et al. Molecular-based FRET nanosensor with dynamic ratiometric NIR-IIb fluorescence for real-time in vivo imaging and sensing. *Nano Lett.* **23**, 4548–4556 (2023).
12. Xiao, X. et al. Ultrasound-driven injectable and fully biodegradable triboelectric nanogenerators. *Small Methods* **7**, 2201350 (2023).
13. Hwang, S. W. et al. Biodegradable elastomers and silicon nanomembranes/nanoribbons for stretchable, transient electronics, and biosensors. *Nano Lett.* **15**, 2801–2808 (2015).
14. Hwang, S. W. et al. 25th anniversary article: materials for high-performance biodegradable semiconductor devices. *Adv. Mater.* **26**, 1992–2000 (2014).
15. Hwang, S. W. et al. A physically transient form of silicon electronics. *Science* **337**, 1640–1644 (2012).
16. Kim, D.-H. et al. Dissolvable films of silk fibroin for ultrathin conformal bio-integrated electronics. *Nat. Mater.* **9**, 511–517 (2010).
17. Dagdeviren, C. et al. Transient, biocompatible electronics and energy harvesters based on ZnO. *Small* **9**, 3398–3404 (2013).
18. Wang, C. H., Hsieh, C. Y. & Hwang, J. C. Flexible organic thin-film transistors with silk fibroin as the gate dielectric. *Adv. Mater.* **23**, 1630–1634 (2011).
19. Imani, I. M. et al. Ultrasound-driven on-demand transient triboelectric nanogenerator for subcutaneous antibacterial activity. *Adv. Sci.* **10**, 2204801 (2023).
20. Hinchet, R. et al. Transcutaneous ultrasound energy harvesting using capacitive triboelectric technology. *Science* **365**, 491–494 (2019).
21. Liu, Y. et al. Engineered magnetic polymer nanoparticles can ameliorate breast cancer treatment inducing pyroptosis-starvation along with chemotherapy. *ACS Appl. Mater. Interfaces* **14**, 42541–42557 (2022).
22. Wong, C. et al. Multistage nanoparticle delivery system for deep penetration into tumor tissue. *PNAS* **108**, 2426–2431 (2011).
23. Zhao, D. et al. Theranostic micelles combined with multiple strategies to effectively overcome multidrug resistance. *Nanomedicine* **13**, 1517–1533 (2018).
24. Oh, K. S. et al. Docetaxel-loaded multilayer nanoparticles with nanodroplets for cancer therapy. *Int. J. Nanomed.* **11**, 1077 (2016).
25. Kim, S., Diab, R., Joubert, O., Carilho, N. & Pasc, A. Core-shell microcapsules of solid lipid nanoparticles and mesoporous silica for enhanced oral delivery of curcumin. *Colloid Surf. B* **140**, 161–168 (2016).
26. Zhang, X., Achazi, K. & Haag, R. Boronate cross-linked ATP-and pH-responsive nanogels for intracellular delivery of anticancer drugs. *Adv. Health Mater.* **4**, 585–592 (2015).
27. Timin, A. S. et al. Cell-based drug delivery and use of nano-and microcarriers for cell functionalization. *Adv. Health Mater.* **7**, 1700818 (2018).
28. Pierigè, F., Serafini, S., Rossi, L. & Magnani, M. Cell-based drug delivery. *Adv. Drug Deliv. Rev.* **60**, 286–295 (2008).
29. Gao, W. et al. Surface functionalization of gold nanoparticles with red blood cell membranes. *Adv. Mater.* **25**, 3549–3553 (2013).
30. Nehoff, H., Parayath, N. N., Domanovitch, L., Taurin, S. & Greish, K. Nanomedicine for drug targeting: strategies beyond the enhanced permeability and retention effect. *Int. J. Nanomed.* **9**, 2539–2555 (2014).
31. Rao, L. et al. Microfluidic electroporation-facilitated synthesis of erythrocyte membrane-coated magnetic nanoparticles for enhanced imaging-guided cancer therapy. *ACS Nano* **11**, 3496–3505 (2017).
32. Sun, X., Wang, C., Gao, M., Hu, A. & Liu, Z. Remotely controlled red blood cell carriers for cancer targeting and near-infrared light-triggered drug release in combined photothermal-chemotherapy. *Adv. Funct. Mater.* **25**, 2386–2394 (2015).
33. Kinoshita, K. Jr & Tsong, T. Y. Formation and resealing of pores of controlled sizes in human erythrocyte membrane. *Nature* **268**, 438–441 (1977).
34. Skorb, E. V. & Möhwald, H. 25th anniversary article: dynamic interfaces for responsive encapsulation systems. *Adv. Mater.* **25**, 5029–5043 (2013).
35. Yu, G. T. et al. Myeloid-derived suppressor cell membrane-coated magnetic nanoparticles for cancer theranostics by inducing macrophage polarization and synergizing immunogenic cell death. *Adv. Funct. Mater.* **28**, 1801389 (2018).
36. Neumann, E., Kakorin, S. & Toensing, K. Membrane electroporation and electromechanical deformation of vesicles and cells. *Faraday Discuss.* **111**, 111–125 (1999).
37. Yarmush, M. L., Golberg, A., Serša, G., Kotnik, T. & Miklavčič, D. Electroporation-based technologies for medicine: principles, applications, and challenges. *Annu. Rev. Biomed. Eng.* **16**, 295–320 (2014).
38. Fonseca, A. C., Gil, M. H. & Simoes, P. N. Biodegradable poly (ester amide)s—a remarkable opportunity for the biomedical area: review on the synthesis, characterization and applications. *Prog. Polym. Sci.* **39**, 1291–1311 (2014).
39. Gross, R. A. & Kalra, B. Biodegradable polymers for the environment. *Science* **297**, 803–807 (2002).
40. Wang, Z. L., Chen, J. & Lin, L. Progress in triboelectric nanogenerators as a new energy technology and self-powered sensors. *Energy Environ. Sci.* **8**, 2250–2282 (2015).
41. Drumright, R. E., Gruber, P. R. & Henton, D. E. Polylactic acid technology. *Adv. Mater.* **12**, 1841–1846 (2000).
42. Athanasiou, K. A., Niederauer, G. G., Agrawal, C. & Sterilisation, T. Biocompatibility and clinical applications of polylactic acid/polyglycolic acid copolymers. *Biomaterials* **17**, 93–102 (1996).
43. Chen, J. et al. Harmonic-resonator-based triboelectric nanogenerator as a sustainable power source and a self-powered active vibration sensor. *Adv. Mater.* **25**, 6094–6099 (2013).
44. Lin, Z. H., Cheng, G., Lin, L., Lee, S. & Wang, Z. L. Water-solid surface contact electrification and its use for harvesting liquid-wave energy. *Angew. Chem. Int. Ed.* **52**, 12545–12549 (2013).
45. Wang, S., Lin, L. & Wang, Z. L. Triboelectric nanogenerators as self-powered active sensors. *Nano Energy* **11**, 436–462 (2015).
46. Zhang, X. S. et al. Frequency-multiplication high-output triboelectric nanogenerator for sustainably powering biomedical microsystems. *Nano Lett.* **13**, 1168–1172 (2013).
47. Zheng, Q. et al. In vivo powering of pacemaker by breathing-driven implanted triboelectric nanogenerator. *Adv. Mater.* **26**, 5851–5856 (2014).
48. Jian, G. et al. Enhanced performances of triboelectric nanogenerators by filling hierarchical flower-like TiO₂ particles into polymethyl methacrylate film. *Nanoscale* **12**, 14160–14170 (2020).
49. Jian, G. et al. Hybrid PDMS-TiO₂-stainless steel textiles for triboelectric nanogenerators. *Chem. Eng. J.* **417**, 127974 (2021).
50. Jian, G. et al. Superhigh charge density and direct-current output in triboelectric nanogenerators via peak shifting modified charge pumping. *Nano Energy* **102**, 107637 (2022).
51. Zhang, C., Tang, W., Han, C., Fan, F. & Wang, Z. L. Theoretical comparison, equivalent transformation, and conjunction operations of electromagnetic induction generator and triboelectric nanogenerator for harvesting mechanical energy. *Adv. Mater.* **26**, 3580–3591 (2014).
52. Zheng, Q. et al. Biodegradable triboelectric nanogenerator as a life-time designed implantable power source. *Sci. Adv.* **2**, e1501478 (2016).
53. Millán, C. G., Castañeda, A. Z., Marinero, M. L. S. & Lanao, J. M. Factors associated with the performance of carrier erythrocytes obtained by hypotonic dialysis. *Blood Cell. Mol. Dis.* **33**, 132–140 (2004).